

PAPER

## Facile approach to fabricate BCN/Fe<sub>x</sub>(B/C/N)<sub>y</sub> nano-architectures with enhanced electromagnetic wave absorption

To cite this article: Tao Zhang *et al* 2018 *Nanotechnology* **29** 235701

View the [article online](#) for updates and enhancements.

### Related content

- [Porous-carbon-nanotube decorated carbon nanofibers with effective microwave absorption properties](#)

Tao Zhang, Bo Xiao, Pengyu Zhou *et al.*

- [Carboxyl multiwalled carbon nanotubes modified polypyrrole \(PPy\) aerogel for enhanced electromagnetic absorption](#)

Kun Zhang, Aming Xie, Fan Wu *et al.*

- [Electromagnetic wave absorption properties of cement based composites using helical carbon fibers as absorbent](#)

Shuai Xie, Jing Wang, Wufeng Wang *et al.*

The advertisement features the Lake Shore Cryotronics logo on the left, showing a blue square icon followed by the company name "Lake Shore" and "CRYOTRONICS". On the right, there is a large image of a probe station with various mechanical components and a circular probe head. To the right of the image, the text reads: "For early-stage material and device research" and "Explore the benefits of cryogenic device probing". A small orange play button icon is located in the bottom right corner of the ad area.

# Facile approach to fabricate BCN/Fe<sub>x</sub>(B/C/N)<sub>y</sub> nano-architectures with enhanced electromagnetic wave absorption

Tao Zhang<sup>1</sup>, Jian Zhang<sup>1</sup>, Heng Luo<sup>2,6</sup>, Lianwen Deng<sup>2</sup>, Pengyu Zhou<sup>3</sup>, Guangwu Wen<sup>1,4</sup>, Long Xia<sup>1,6</sup>, Bo Zhong<sup>1</sup> and Haibin Zhang<sup>5</sup>

<sup>1</sup> School of Materials Science and Engineering, Harbin Institute of Technology (Weihai), Weihai 264209, People's Republic of China

<sup>2</sup> School of Physics and Electronics, Institute of Super-microstructure and Ultrafast Process in Advanced Materials, Central South University, Changsha, 410083, People's Republic of China

<sup>3</sup> Department of Mechanical Engineering, The Hong Kong Polytechnic University, Kowloon, Hong Kong

<sup>4</sup> School of Materials Science and Engineering, Shandong University of Technology, 255049, People's Republic of China

<sup>5</sup> Innovation Research Team for Advanced Ceramics, Institute of Nuclear Physics and Chemistry, China Academy of Engineering Physics, Mianyang 621900, People's Republic of China

E-mail: [luohengcsu@csu.edu.cn](mailto:luohengcsu@csu.edu.cn) and [xialonghit@gmail.com](mailto:xialonghit@gmail.com)

Received 5 December 2017, revised 20 February 2018

Accepted for publication 8 March 2018

Published 9 April 2018



## Abstract

Carbon-based materials have excited extensive interest for their remarkable electrical properties and low density for application in electromagnetic (EM) wave absorbents. However, the processing of heteroatoms doping in carbon nanostructures is an insuperable challenge for attaining effective reflection loss and EM matching. Herein, a facile method for large-scale synthesis of boron and nitrogen doped carbon nanotubes decorated by ferrites particles is proposed. The BCN nanotubes (50–100 nm in diameter) imbedded with nanosized Fe<sub>x</sub>(B/C/N)<sub>y</sub> (10–20 nm) are successfully constructed by two steps of polymerization and carbonthermic reduction. The product exhibits an outstanding reflection loss (RL) performance, in that the minimum RL is –47.97 dB at 11.44 GHz with a broad bandwidth 11.2 GHz (from 3.76 to 14.9 GHz) below –10 dB indicating a competitive absorbent in stealth materials. Crystalline and theoretical studies of the absorption mechanism indicate a unique dielectric dispersion effect in the absorbing bandwidth.

Keywords: borocarbonitride, nanotubes, electromagnetic wave absorption

(Some figures may appear in colour only in the online journal)

## 1. Introduction

It is widely acknowledged that electromagnetic (EM) wave absorbing materials play important roles both in defense-oriented and commercial applications, especially in the waveband of gigahertz [1, 2]. Metal powders and ferrite have been demonstrated to be practical EM wave absorbing/shielding materials at early stage of development [3, 4]. Driven by the demand for high attenuation coefficient as well as adequate absorbing bandwidth, more and more efforts have

been devoted to exploring new types of efficient absorbing materials.

In the past few decades, in the basis of technological advances in microstructural control at nanoscale, many experimental results have proved that carbon-based nanomaterials with superior specific surface and quantum tunneling effect, such as carbon nanotubes and carbon nanofibers, are favorable EM wave absorbers [5–8]. It should be noted here that incorporation of B or/and N into carbon-based nanomaterials, namely borocarbonitride (BCN), could provide additional loss mechanism of polarization relaxation due to the lattice defects or vacancy [9–11]. Actually, as an advanced functional material, BCN nanomaterials

<sup>6</sup> Authors to whom any correspondence should be addressed.

have been widely studied as functional or/and structural materials, involving thin films [12, 13], nanoflakes/nanosheets [14–16], nanotubes [17, 18], particles [19], wires/fibers [20], coatings (including surface coating and interphase of composites) [9, 15] and blocks [6, 21]. Additionally, owing to their excellent dielectric-tunable property, low density, oxidation resistance, chemical stability, BCN based architectures are expected to be the promising candidate of EM wave absorbing materials [9, 21–23]. Specifically, BCN based nanotubes with strong anisotropy are considered to act as micro-dipoles which accelerated the conversion of EM energy into heat efficiently [17, 18]. Meanwhile, hexagonal ternary BCN materials have aroused extensive interests owing to their low density, multiple-layered structure and semiconductor property [24]. Hexagonal BCN architectures with variable compositions were researched and prepared by various methods. For example, Kang *et al* introduced B and N atoms into graphene to fabricate BCN nanosheets with enhanced EM wave absorption performances [9]. Huang *et al* fabricated hexagonal BCN via high-temperature calcination at 1250 °C, the products exhibited tunable electrical properties between BN nanosheets and graphene [10]. Ma *et al* prepared ternary BCN nanosheets through thermal substitution at 850 °C from a mixture of graphene and BN nanosheets, the architecture showed controllable nonlinear optical performance [25].

However, these methods require complicated processes and conditions for BCN synthesis. Herein, we propose a facile approach through pyrolysis of melamine-formaldehyde-boronic acid compound catalyzed by Fe<sup>3+</sup> to fabricate BCN/Fe<sub>x</sub>(B/C/N)<sub>y</sub> nano-architectures for enhanced EM wave absorption. Effects of annealing temperature on the microstructural characteristics and composition distributions of as-prepared BCN/Fe<sub>x</sub>(B/C/N)<sub>y</sub> structures are investigated in detail. Additionally, obvious EM wave dielectric dispersion effect and tunable absorbing performance are discussed. These findings point to important guidelines to take advantages of functionalized BCN nano-structure absorber

and pave the way for the development of a large family of novel structure EM wave absorbing materials.

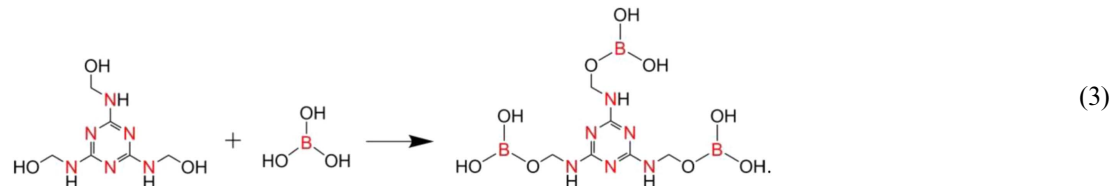
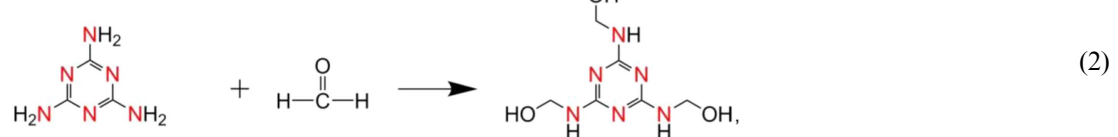
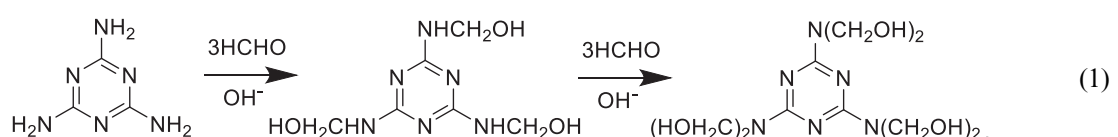
## 2. Experimental

### 2.1. Precursor synthesis

Details of fabrication processes of BCN/Fe<sub>x</sub>(B/C/N)<sub>y</sub> nano-architectures are illustrated in figure 1.

Firstly, 4 g NaOH (analytical reagent, from Cangzhou Shenhao Chemical Products Co., Ltd) solid is dissolved into 100 ml deionized water forming a solution with concentration of 1 mol l<sup>-1</sup>. Then, 16 ml formaldehyde solution (37 wt%, 0.2 mol, from Shanghai Yuqin Chemical Co., Ltd) is diluted with 150 ml deionized water whose pH value is adjusted at the range of 8–9 by the prepared NaOH solution with the assistance of magnetic stirrer in room temperature. After that, the formaldehyde solution is heated to 80 °C. Then, 8 g melamine (0.064 mol, analytical reagent, from Suzhou Pengbo Fine Chemical Co., Ltd) and 3.6 g boric acid (0.06 mol, analytical reagent, from Nanjing Chemical Reagent Co., Ltd) are introduced into the formaldehyde solution forming a transparent solution at 80 °C. 1 g FeCl<sub>3</sub> · 6H<sub>2</sub>O (0.0037 mol, analytical reagent, from Shanghai Zhanyun Chemical Co., Ltd) is added into the above solution and elevate the temperature to 90 °C for 30 min producing the bright orange precipitate. At last, the precipitate is collected and dried at 180 °C for 12 h in a vacuum drying-oven to gain a sufficiently cross-linked precursor. The first advantage of the method mentioned in the manuscript is that the precursor can be stably produced in large scale. The second advantage is that the synthesis process is environmental-friendly which is free from the usage of toxic chemical reagents.

The possible reaction equations between melamine, formaldehyde and boric acid are shown as follows:



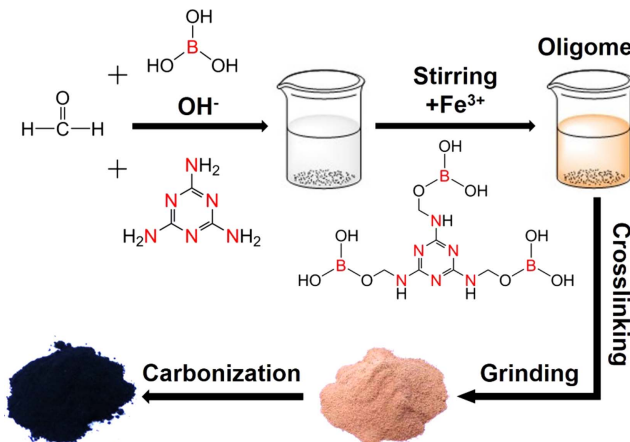


**Figure 1.** Fabrication process of BCN/Fe<sub>x</sub>(B/C/N)<sub>y</sub> nano-architectures.

**Table 1.** Pyrolysis programs for the BCN precursors.

Sample No.	Max temperature/°C	Soaking time at max temperature/h
1	950	2.0
2	1050	0.5
3	1050	1.0
4	1050	2.0
5	1150	2.0

## 2.2. Pyrolysis of the precursor

Firstly, the prepared precursor is manually ground by a ceramic mortar to obtain a fine powder (about 200–300 meshes). Secondly, the precursor powder is loaded into an alumina crucible and heated to different temperatures in a tube furnace protected by flowing nitrogen atmosphere (purity 99.99%) with a heating rate of 10 °C min<sup>-1</sup>. At last, after the furnace cooling down to room temperature naturally, the products are collected from the crucibles without any further purification. The as-prepared products are the BCN/Fe<sub>x</sub>(B/C/N)<sub>y</sub> nano-architectures exhibiting black and fluffy morphology. The molecule chains of precursor are crosslinked and form a thermosetting shell with the assistance of high temperature. Small volatile molecules and function groups such as –BO, –NH<sub>2</sub>, –NH, and –CH<sub>2</sub> could release from the precursor which would act as the B, C and N sources to form BCN nanotubes. In the crosslinked powder, iron would catalyze these small molecules to grow BCN nanotubes during the cooling stage in the furnace. The pyrolysis parameters are listed in table 1.

## 2.3. Characterization

The phase analysis was performed on x-ray diffraction (XRD, D/max 2550, Japan). The micro-morphologies were characterized by a Nova Nano SEM 230 field-emission scanning electron microscopy (SEM) and a HT7700 transmission electron microscopy (TEM). Raman spectroscopy (Renishaw, RM-1000) was performed to research the structure characteristics. The chemical characteristics of the products were

examined using x-ray photoelectron spectroscopy (XPS, Physical Electronics PHI 5700 with Mg exciting source). For the studies of EM wave absorbing properties of the BCN nano-architectures, the measurement for EM parameters were conducted on a network analyzer (Agilent 5230 A) in the frequency ranging from 2 to 18 GHz by the coaxial line method. The BCN composites were homogeneously dispersed into paraffin. The mass ratio of paraffin and BCN nanomaterial is 3:1 shaping into concentric rings with an outer diameter of 7.0 mm, inner diameter of 3.0 mm and thickness of 2.0 mm, respectively. According to the transmission line theory, the reflection loss (RL) curves with different thickness were calculated by the following equations:

$$RL(dB) = 20 \log \left| \frac{Z_{in} - 1}{Z_{in} + 1} \right| \quad (4)$$

$$Z_{in} = \sqrt{\frac{\mu_r}{\epsilon_r}} \tanh \left[ j \frac{2\pi f d}{c} \sqrt{\mu_r \epsilon_r} \right], \quad (5)$$

where Z<sub>in</sub> refers to input impedance, j is the imaginary unit (i.e. equals to  $\sqrt{-1}$ ), c is the velocity of EM waves in free space, f is the EM wave frequency, and d is the thickness of the samples. A MATLAB code was developed to extract the effect of thickness and frequency on the RL.

## 3. Results and discussion

The BCN/Fe<sub>x</sub>(B/C/N)<sub>y</sub> physical and chemical architectures are artfully designed by pyrolyzed the precursor to enhance the ability of EM wave absorption. Conductive BCN nanotubes (diameter: 50–100 nm; length: 3–5 μm) with ferrite nano-dots on the cap of the BCN nanotubes, are used as absorbing units. The Fe<sub>x</sub>(B/C/N)<sub>y</sub> shells wrapped on the BCN nanotubes are used as dielectric units and the wrinkled Fe<sub>x</sub>(B/C/N)<sub>y</sub> shells (which grow with a few BCN nanotubes) with paraffin are impedance matching units. A schematic illustration of the architecture is shown in figure 2.

Figure 3 shows a group of SEM images of the BCN/Fe<sub>x</sub>(B/C/N)<sub>y</sub> nano-architectures annealed at different temperatures and holding time. A large number of curved nanotubes wrapped by irregular dense shell can be clearly observed from figures 3(a) and (b). The thickness of the shell is about 1–2 μm with an irregular polyhedral structure when products annealed at 950 °C for 2 h. The polyhedral dense shell becomes more regular and the wrapped nanotubes grow larger when the temperature increases to 1050 °C (figures 3(c) and (d)). The shell thickness is less than 1 μm much thinner than the sample annealed at lower temperature. The diameter of the nanotubes which randomly distribute in the polyhedral shell is about 200–300 nm larger than the above sample annealed at lower temperature. When the temperature increases to 1150 °C for 2 h, the polyhedral shells almost disappear. The spherical architecture (2 μm in diameter) with few nanotubes and nano-flakes grown on the surface are observed according to figures 3(e) and (f) due to the unstable chemical composition of the shell.

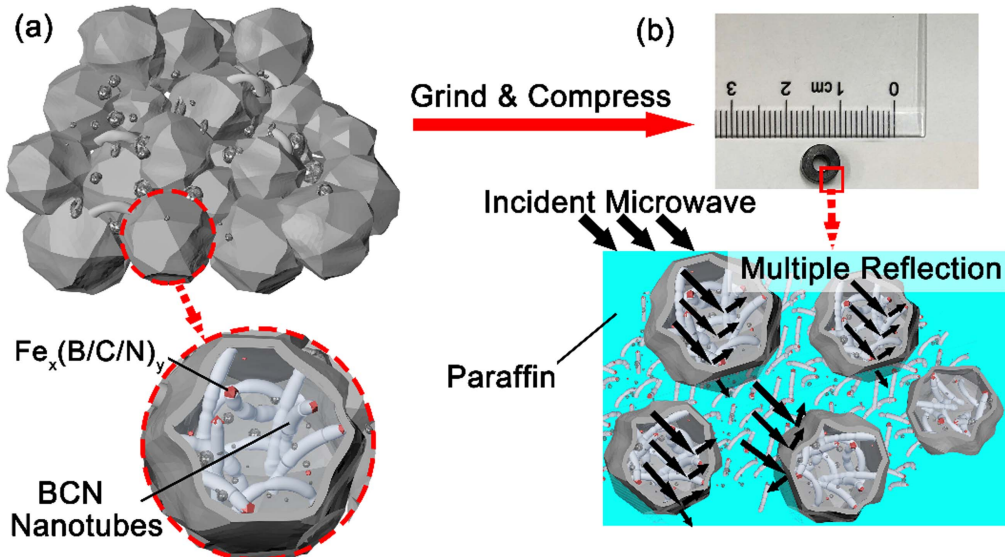


**Figure 2.** (a) The nano-architecture of the BCN/Fe<sub>x</sub>(B/C/N)<sub>y</sub> absorbent, (b) the EM testing ring and the microscopic composition of concentric rings.

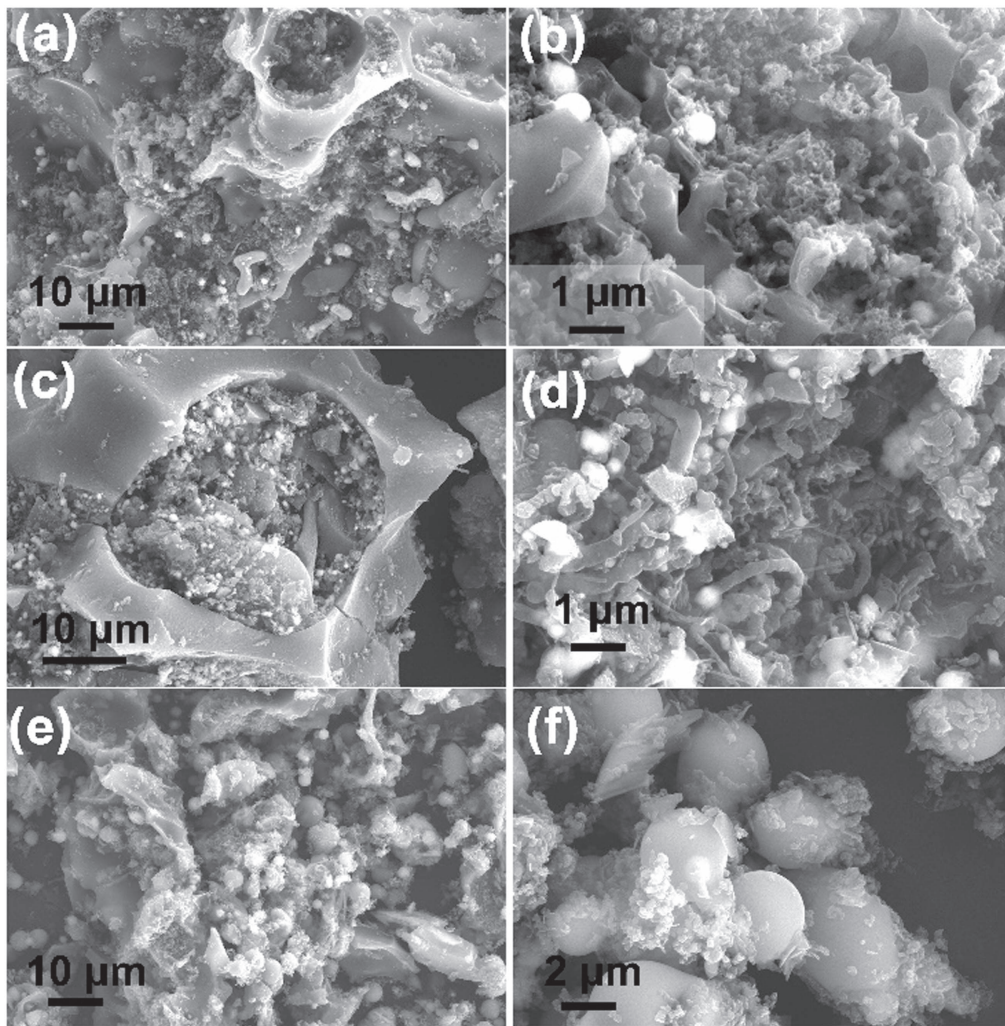


**Figure 3.** SEM images of the BCN/Fe<sub>x</sub>(B/C/N)<sub>y</sub> nano-architectures annealed for 2 h at (a), (b) 950 °C, (c), (d) 1050 °C, and (e), (f) 1150 °C.

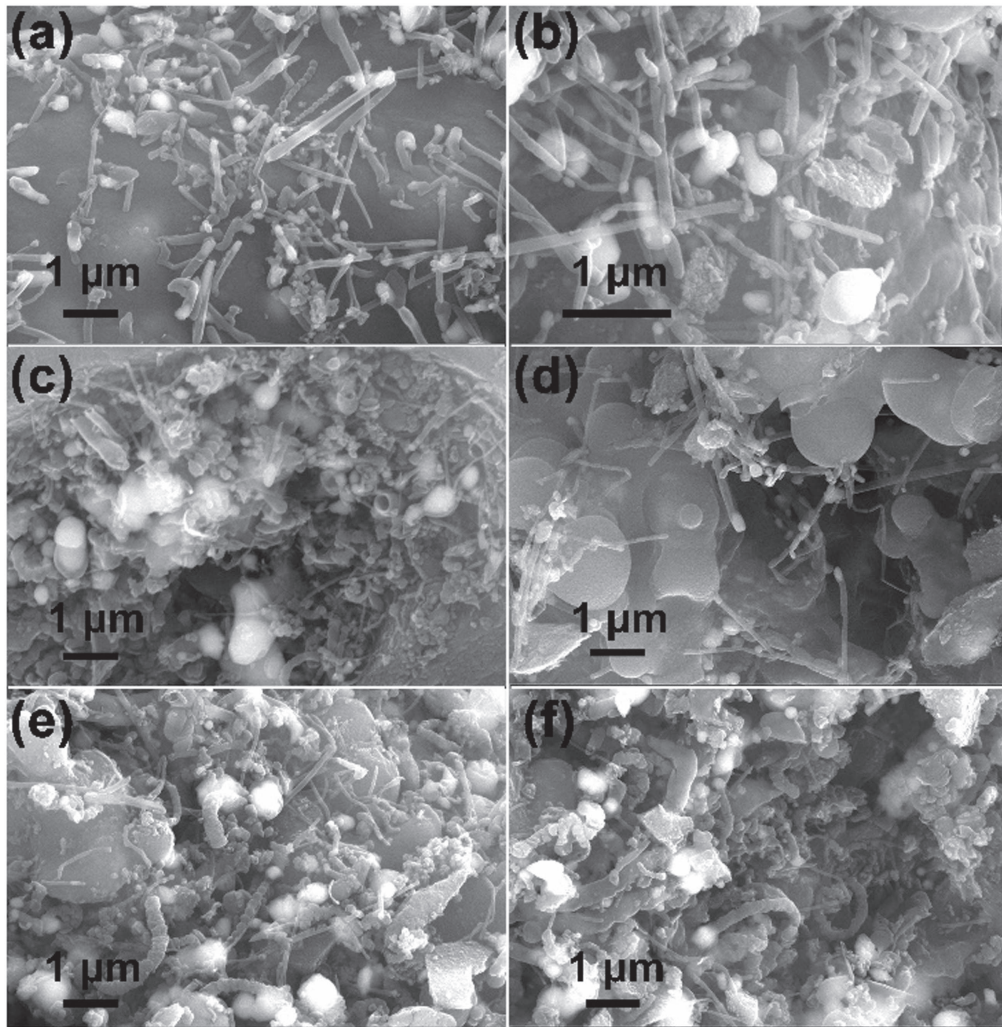


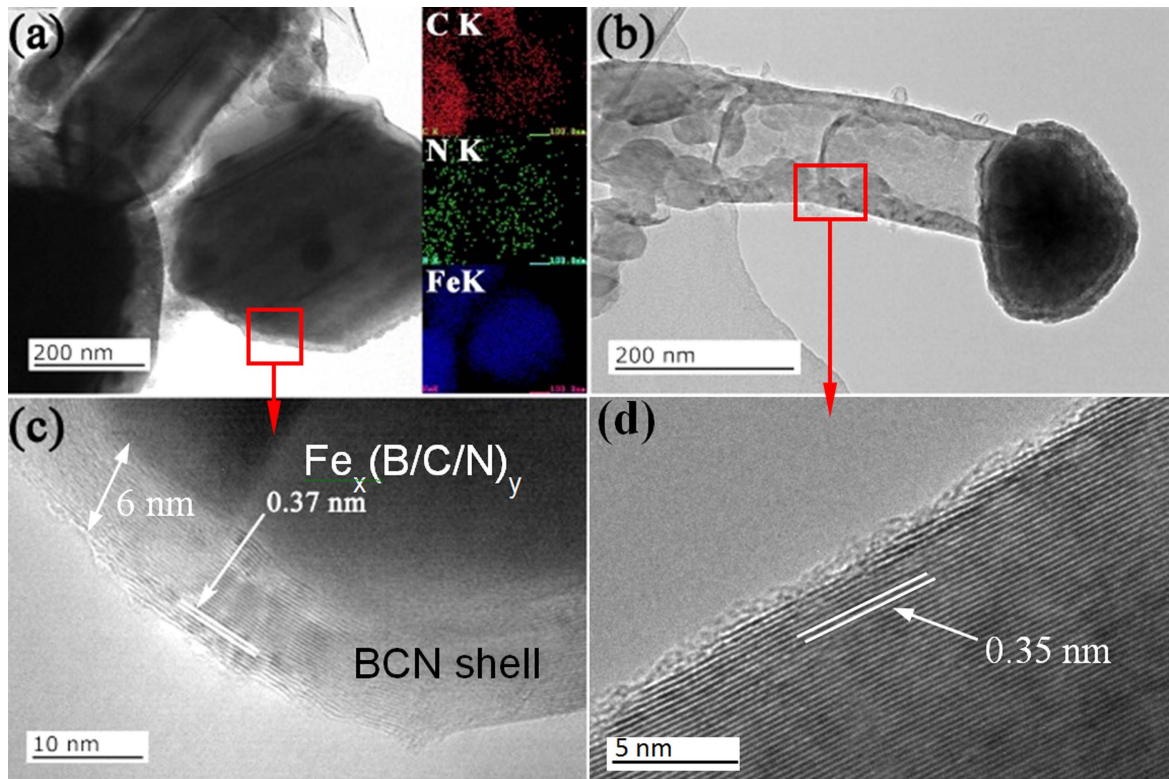
**Figure 4.** SEM images of BCN ceramics after pyrolysis at 1050 °C for (a), (b) 0.5 h, (c), (d) 1 h, and (e), (f) 2 h.

The morphology and diameter of the BCN nanotubes prepared with different holding time at 1050 °C are displayed in figure 4. For the BCN nanotubes gained at 1050 °C for 0.5 h show a short-stick like morphology with length to diameter ratio about 8 and with the ferrite nano-dot on the tip (diameter: about 150 nm). The BCN nanotubes of the as-prepared BCN/Fe<sub>x</sub>(B/C/N)<sub>y</sub> nano-architectures obtained at 1050 °C for 1 h are more uniform with diameter about 150 nm also with a ferrite nano-dot on the tip (figures 4(c) and (d)). When the holding time increases to 2 h at 1050 °C, the morphology of BCN nanotubes becomes curly and the diameter increases to about 300 nm. It should be notice that the increase of holding time from 0.5 to 2 h, the average diameters of the BCN nanotubes increase from 100 nm at 0.5 h to 300 nm at 2 h. Moreover, the polyhedral shells wrapped on the BCN nanotubes disappear when the holding time reach to 2 h (figures 4(e) and (f)). Such observations provide a clear relationship among the size of BCN nanotubes, the existence of the polyhedral shells and the annealing time. The *in situ* growth of the BCN nanotubes in the polyhedral shells agrees with the typical nucleation-growth model, in which BCN nanotubes nucleate on the catalytic Fe<sup>3+</sup> regions and then

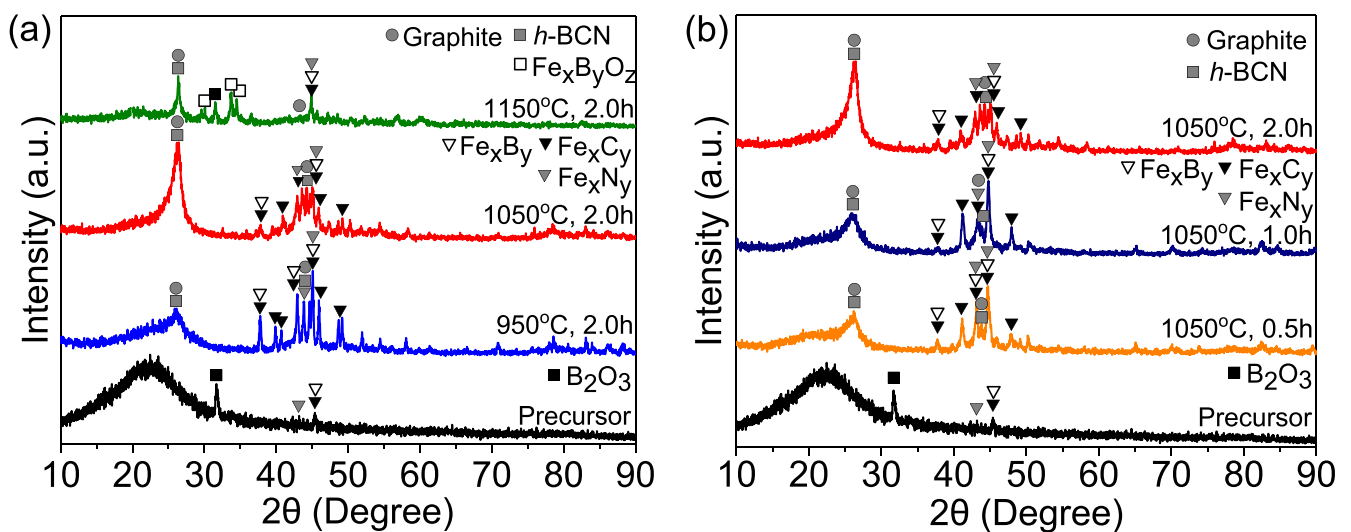
grow into larger hexagonal structure tubes on the shell substrate [26–28].

Figure 5(a) displays a TEM image of a BCN/Fe<sub>x</sub>(B/C/N)<sub>y</sub> nano-structural composite. The energy dispersive spectrometer (EDS) mappings of C, N and Fe suggest the homogeneous element distribution in the nano-architecture. B element is not identified just because of the detector limitation of EDS. Figure 5(b) shows a single BCN nanotube decorated with a Fe<sub>x</sub>(B/C/N)<sub>y</sub> nano-particle cap. The Fe<sub>x</sub>(B/C/N)<sub>y</sub> nano-particle is warped by a thin layer of hexagonal BCN shell (about 6 nm in thickness) which has a interplanar spacing of 0.37 nm according to HRTEM image shown in figure 5(c). The BCN nanotube exhibits the wall thickness about tens of nanometers and the clear lattice fringes with an interplanar spacing about 0.35 nm (figure 5(d)).

Figure 6 shows the XRD patterns of the as-prepared BCN/Fe<sub>x</sub>(B/C/N)<sub>y</sub> nano-structures annealed at different temperatures and holding time. The broad peak at about 22° suggests the typical amorphous structure of the precursor substrate (black curve). The peaks at 32.2° is corresponding to (003) planes of B<sub>2</sub>O<sub>3</sub> (JCPDS no. 06-0634). The diffraction peaks and relative intensities match well with the standard



**Figure 5.** (a) The low and (b) the high magnification TEM images of the as-prepared BCN/Fe<sub>x</sub>(B/C/N)<sub>y</sub> nano-architectures, HRTEM images of (c) the spherical Fe<sub>x</sub>(B/C/N)<sub>y</sub> terminals and (d) the wall of BCN nanotubes.



**Figure 6.** XRD patterns of as-prepared BCN/Fe<sub>x</sub>(B/C/N)<sub>y</sub> nano-architectures annealed at (a) different temperatures and (b) holding time.

XRD data of hexagonal BCN (JCPDS no. 35-1292), and the diffraction peak at 26.0° is associated with the (002) planes of h-BCN when the precursor annealed at different temperatures and holding time. When the precursor is heated from 950 °C to 1150 °C, the amorphous substrate gradually disappears and the typical peaks of hexagonal BCN (26.0°, JCPDS no. 35-1292) become sharp. Moreover, the intensity of characteristic peaks of Fe<sub>x</sub>N<sub>y</sub> (JCPDS no. 85-0871, 72-1110, 36-1248 and 51-0997) and Fe<sub>x</sub>C<sub>y</sub> (JCPDS no. 83-0877, 73-2101, 17-0333, 72-2126 and 73-2102) are increased with higher annealing

temperature; additionally, it is noteworthy that Fe<sub>3</sub>C and Fe<sub>3</sub>N exhibit preponderant phases in the as-prepared samples annealed at 1050 °C. Graphite phase is also detected at 26.38° and 44.39° (JCPDS no. 41-1487) revealing the hybrid substrate which could function as shielding unit for the incident EM wave. Figure 6(b) shows the XRD patterns of the precursor annealed at 1050 °C for 0.5, 1, and 2 h, respectively. The characteristic peak of h-BCN and graphite at around 26° becomes sharp and shifts to higher diffraction angles suggesting that there is better crystallization with increasing

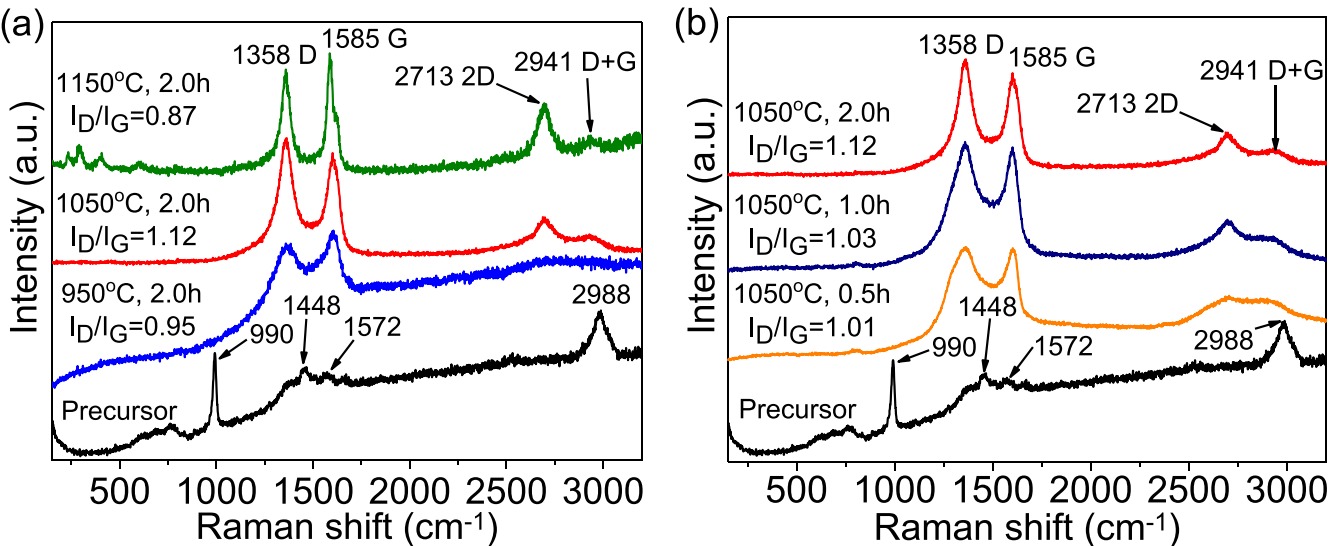


**Figure 7.** Raman shifts of as-prepared BCN/Fe<sub>x</sub>(B/C/N)<sub>y</sub> nano-architectures annealed at (a) different temperatures and (b) different holding time.

holding time. The amorphous broad peak of the precursor at 22° almost disappears at 1050 °C for 0.5 h. The peak intensity of the phases of Fe<sub>x</sub>C<sub>y</sub>, Fe<sub>x</sub>N<sub>y</sub>, and Fe<sub>x</sub>B<sub>y</sub> increases with longer holding time indicating that the diffusion speed of B, C and N atoms into iron is controlled by the holding time. No additional peaks belonging to impure phases are detected, suggesting the good crystallinity and purity of the products.

The Raman spectra (figure 7) recorded with the 532 nm wavelength excitation indicate that the BCN/Fe<sub>x</sub>(B/C/N)<sub>y</sub> nano-architectures show characteristic D-, G-bands at 1358 cm<sup>-1</sup> and 1585 cm<sup>-1</sup> respectively which have lower wave number comparing with graphite (the characteristic D- and G-bands of graphite are about 1345 cm<sup>-1</sup> and 1578 cm<sup>-1</sup>, respectively [29]). The red-Raman-shift phenomenon of the samples reveals the existence of B and N dopants in hexagonal C-C structures [11, 30]. The G-band is attributed to the stretching of all sp<sup>2</sup>-bonded pairs of C-C, B-C-N bonding. D-band is related to the sp<sup>3</sup> defects or lattice distortion [11, 27]. The ratio of  $I_D/I_G$  is usually used as a key factor to evaluate the defect density in the carbon based materials. The higher of the factor  $I_D/I_G$  indicates more B and N dopants in graphite structure [11, 31]. The  $I_D/I_G$  increases from 0.95 (annealed at 950 °C for 2 h) to 1.12 (annealed at 1050 °C for 2 h) revealing that the diffusion speed of B and N atoms is accelerated by higher temperature establishing more defects in the B-C-N networks (figure 7(a)). When the temperature reaches to 1150 °C for 2 h, the  $I_D/I_G$  decreases to 0.87 indicating that the diffusion process of B and N atoms almost finished and the crystalline structures are rebuilt. Figure 7(b) shows the Raman curves annealed at 1050 °C for 0.5, 1 and 2 h respectively. The  $I_D/I_G$  increases with longer holding time at 1050 °C indicating the diffusion effects at that temperature which mechanism agrees well with the structure evolution shown in figure 7(a). The Raman spectrum of the precursor shown both in figures 7(a) and (b) exhibits a sharp peak at 900 cm<sup>-1</sup> owing to the breathing mode of borazine

ring according to literature [32]. The C-H bonds in the precursor are also observed at 1448, 1572 and 2988 cm<sup>-1</sup> [33].

It is expected that high  $I_D/I_G$  values means high disorder in carbon materials or even lots of defects. However, we cannot draw a conclusion that this disorder or defects would decrease complex permittivity. Actually, there exists electron migration inside carbon materials when exposed to EM field, which leads to electric charge accumulation at the disorder interfaces and defects. As results, the disorder or defects insides materials could act as a ‘micro-capacitor’ and promote dielectric permittivity which usually referred to as space charge polarization. This enhanced value of permittivity is consistent with that observed for other electroceramics with giant permittivity [34, 35]. Specifically, the majority of the samples prepared at 1050 °C have an unbroken core-shell structure which could increase the amount of micro-capacitor of the composites according to the SEM results. Moreover, the BCN nanotubes prepared at 1050 °C have larger diameters than other two samples prepared at 950 °C and 1150 °C shown in figure 3. The larger diameter of the BCN nanotubes would further decrease the conductivity due to the smaller specific surface (less contact area for electron transportation). Consequently, it is reasonable that the higher  $I_D/I_G$  value of the sample obtained at 1050 °C than the other two.

The XPS spectrum of full range scanning (figure 8(a)) measured the existence of B, C, N, O and Fe in the as-prepared BCN/Fe<sub>x</sub>(B/C/N)<sub>y</sub> nano-architectures. It is reasonable that the BCN nanotubes and Fe<sub>x</sub>(B/C/N)<sub>y</sub> contribute to the composition of B, C and N, and Fe respectively. The atomic ratio of B:C:N:Fe calculated from the XPS spectrum is about 1.00:11.13:1.70:0.07. Oxygen is also observed in the sample due to the moisture absorption in the porous structure. High resolution spectra of B 1s, C 1s and N 1s were simulated by fitting the peaks using the multi-peak Gaussian method (figures 8(b)–(d)). The lower binding energy feature at 189.3 eV could be assigned to B-C binding and the higher binding energy at 190.8 and 191.5 eV could be assigned to

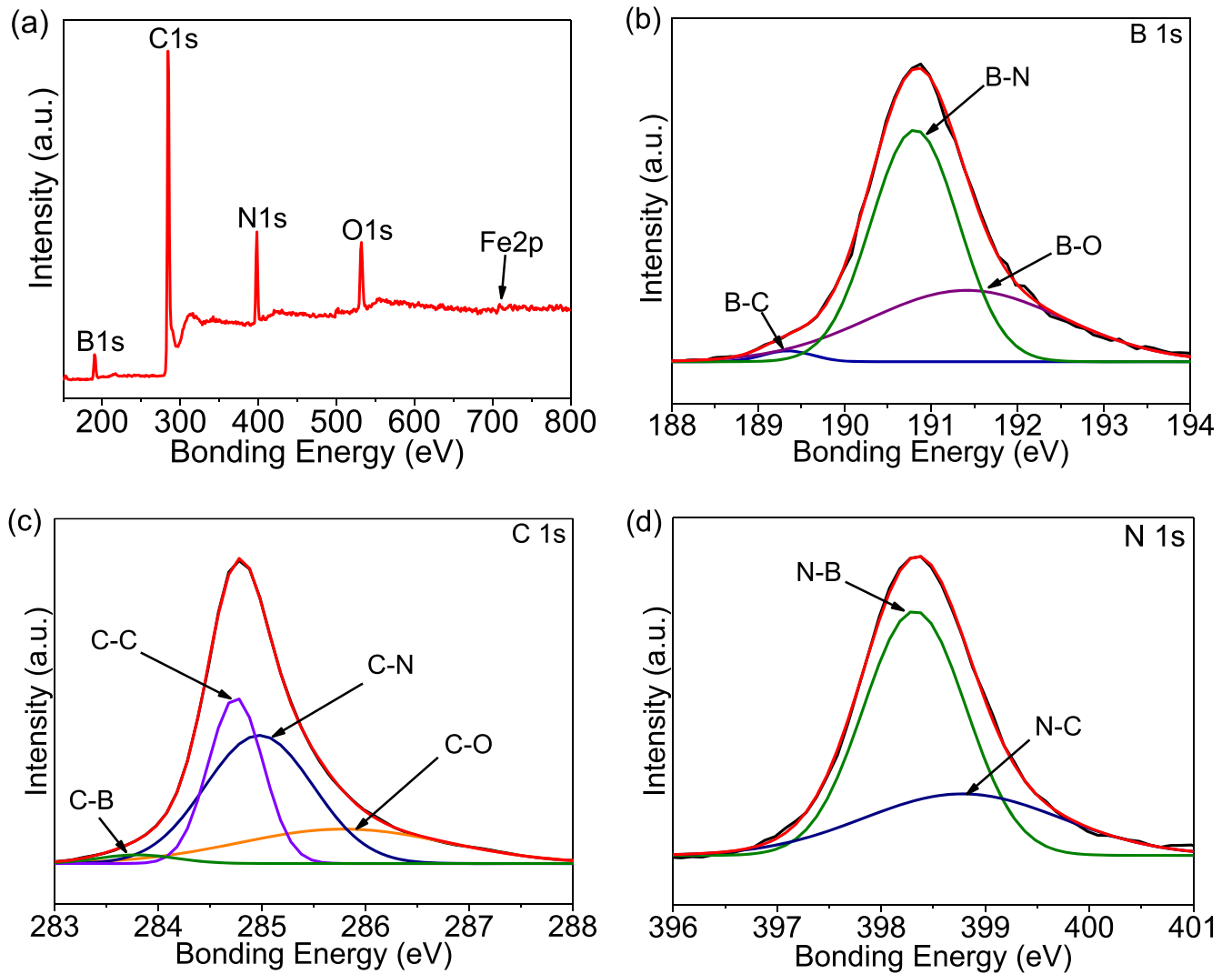


**Figure 8.** XPS spectra of the BCN/Fe<sub>x</sub>(B/C/N)<sub>y</sub> nano-architectures annealed at 1050 °C for 2 h: (a) survey spectra; (b) B 1s peak; (c) C 1s peak; and (d) N 1s peak.

B–N and B–O bindings respectively suggesting the existence of h-BCN and B<sub>2</sub>O<sub>3</sub> [13], which agree well with the XRD results (figure 8(b)). Figure 8(c) shows the C 1s spectrum which includes three fine peaks. The binding energy at 283.8, 284.7, 285.0 and 285.9 eV could be assigned to C–B, C–C, C–N and C–O bindings respectively, revealing the existence of hexagonal BCN hybrid. Figure 8(d) shows the fitting peaks of N 1s spectrum. The binding energy at 398.2 and 398.8 eV could be assigned to N–B and N–C bindings respectively. The XPS results conclusively testify that B and N atoms are successfully doped in graphite structure.

It is well recognized that the vast majority of the EM wave absorbing materials are frequency dependent, and that dependence constrains the values of the real and imaginary parts of the relative permittivity and permeability. As illustrated in figures 9(a) and (b), both real and imaginary parts of permittivity are overall inclined to decrease with increased frequency. It should be noticed that this frequency dependence characteristic is usually referred to frequency dispersion relation and considered to be helpful to enhance attenuation.

Besides, both the real and imaginary parts of permittivity have a general trend of decreasing with increasing in annealing temperature as well, and achieve maximum value when annealed at 1050 °C for 2 h. This enhancement of permittivity could be attributed to the incorporation of polar bonds, or/and even defects, into carbon after B and N doping which has been confirmed by XRD and XPS results. As is known, migration of free electrons located in conductive carbon lattice which were excited by external electric field is responsible for the electric polarization. And this polarization process would be enhanced by the incorporation of polar B–C, N–C bonds and defects, which is also accordance with the increasing in real permittivity. Scattering effect of the defects and polar bonds on repeated migration movement of electrons under alternating EM wave would be enhanced at the same time, giving rise to additional attenuation mechanism and the increment of imaginary permittivity. However, a sharp decrease could be observed when further increases sintering temperature to 1150 °C. This is ascribed to the

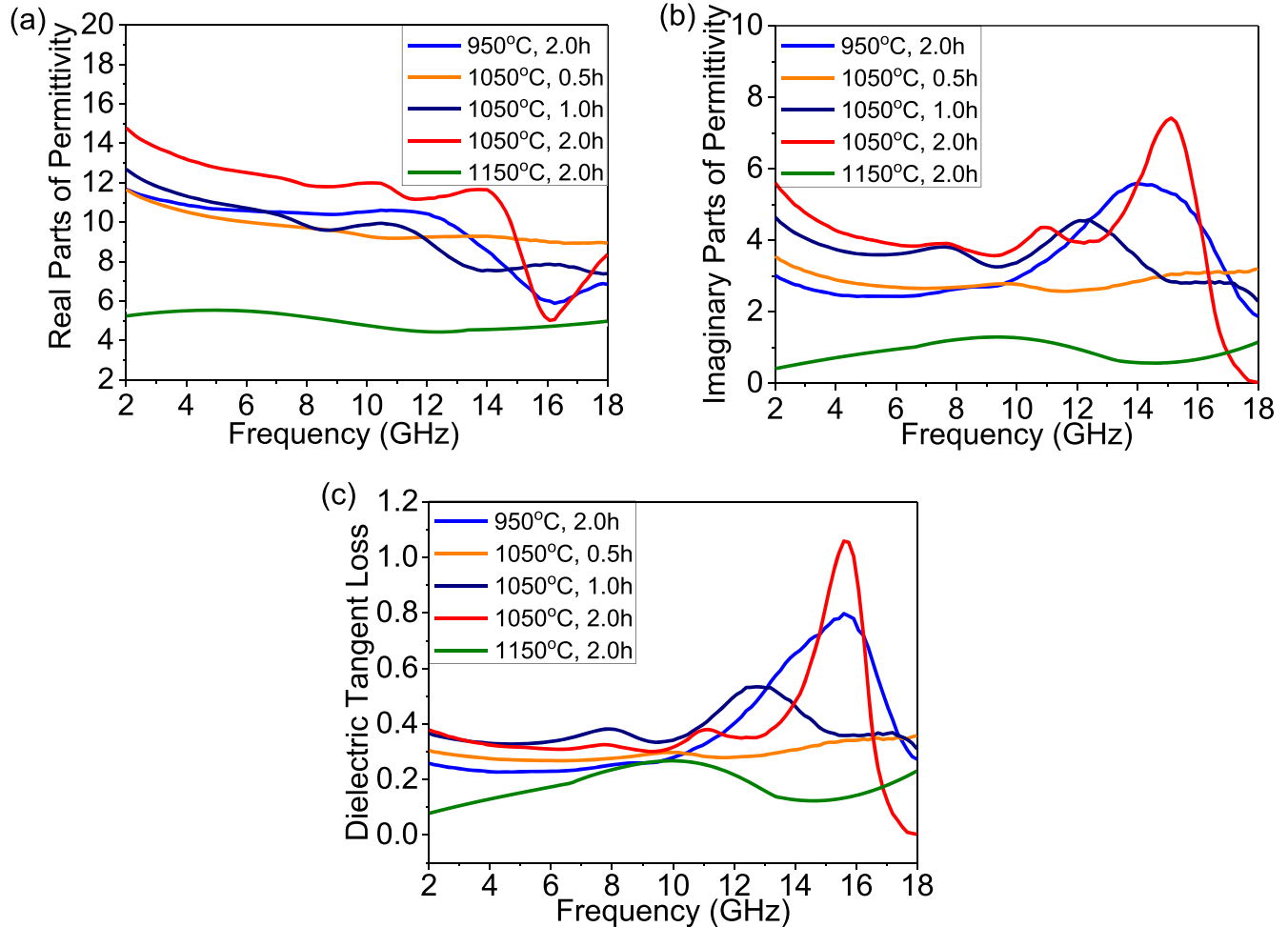


**Figure 9.** EM parameters of the BCN/Fe<sub>x</sub>(B/C/N)<sub>y</sub> nano-architectures: (a) real and (b) imaginary parts (c) dielectric tangent loss of complex permittivity.

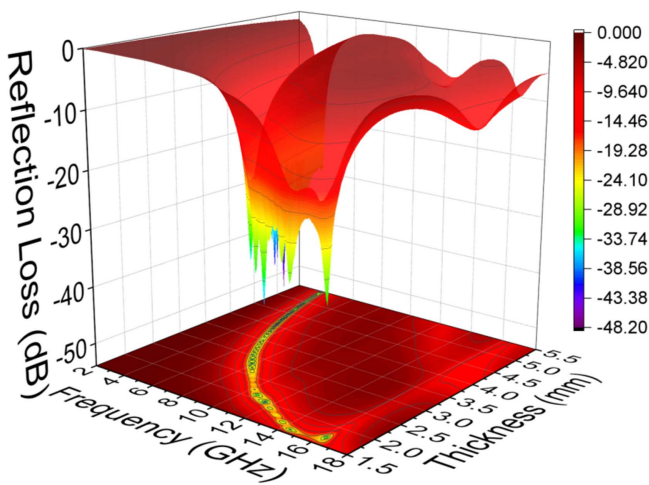


**Figure 10.** 3D plot and contour map of RL value of the BCN/Fe<sub>x</sub>(B/C/N)<sub>y</sub> nano-architectures annealed at 1050 °C for 2 h.

agglomeration of the Fe<sub>x</sub>(B/C/N)<sub>y</sub> shells with vanishment of shielding function unit of the complex nano-structure.

Another important feature is the obvious fluctuation of dielectric spectrum especially the imaginary permittivity over the high frequency range. For clarity, dielectric tangent loss

( $\tan \delta = \epsilon''/\epsilon'$ ) values, which is usually considered to be the typical physics quantity to characterize EM wave absorbing performance, are calculated and shown in figure 9(c). As expected, multi-peaks could be observed, suggesting multiple strong loss mechanisms occurred. This peaked feature could be ascribed to the dielectric relaxation in the hybrid bonding of B–C and N–C. Additionally, hopping migration of electrons among defects also makes contribution to overall EM wave absorbing performance.

To put EM wave absorbing properties of the as-prepared BCN/Fe<sub>x</sub>(B/C/N)<sub>y</sub> nano-architectures into perspective, a three-dimensional plot of effects of frequency and thickness on the calculated RL is shown in figure 10. In the process of calculation, the relative permeability of the BCN/Fe<sub>x</sub>(B/C/N)<sub>y</sub> is set to 1. This is mainly due to the fact that the magnetic response is so weak that could be neglected. As clearly seen in figure 10(a), obvious absorbing peaks could be observed which is in accordance with the dielectric behaviors discussed above. For clarity, a contour map of EM wave RL is illustrated in figure 10 (on the bottom). The results have shown that the optimal values of RL are lower than -30 dB, suggesting more than 99.9% energy of incident EM wave have been dissipated. Besides, a broad coverage of the strong absorbing band ranging

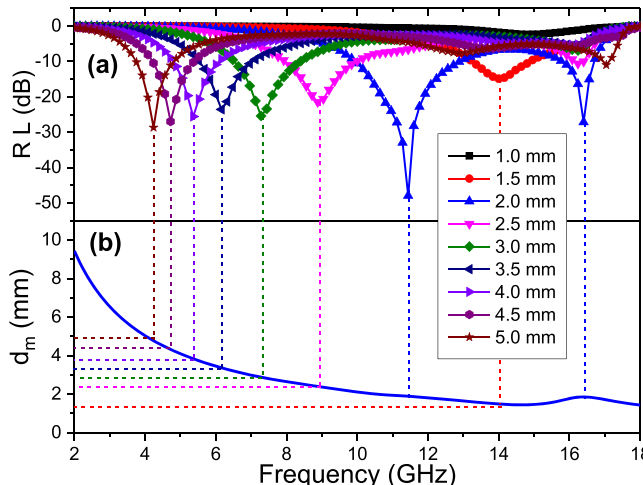


**Figure 11.** (a) RL and (b) frequency-dependence matching thickness of the BCN/Fe<sub>x</sub>(B/C/N)<sub>y</sub> nano-architectures annealed at 1050 °C for 2 h.

from 17 to 4 GHz could be achieved. It should be noticed that the tunable EM wave absorbing performance at low frequency makes the BCN/Fe<sub>x</sub>(B/C/N)<sub>y</sub> nano-architectures more competitive toward practical application.

Figure 11 shows the RL of the BCN/Fe<sub>x</sub>(B/C/N)<sub>y</sub> nano-architectures according to equations (4) and (5) with measured values of  $\varepsilon_r$  and  $\mu_r$ . From figure 11(a), an optimal RL value of -47.9 dB could be reached at 11.44 GHz for the BCN/Fe<sub>x</sub>(B/C/N)<sub>y</sub> and paraffin composites with the thickness of 2 mm. Additionally, the peaked values of RL intend to shift to lower frequency with increasing thickness, suggesting that the range of absorption frequency can be modulated by adjusting the thickness of the samples. According to the resonant absorbing theory, when EM wave is incident on an absorber sample backed by a perfect conductor, the predicted matching thickness  $d_m$  at the matching frequency  $f_m$  is given by:

$$d_m = \frac{nc}{4f_m\sqrt{|\mu_r\varepsilon_r|}}, \quad (6)$$

where  $\mu_r$  and  $\varepsilon_r$  are complex permeability and permittivity at the frequency of  $f_m$ , respectively.  $n$  and  $c$  are the refractive index of EM wave and the velocity of EM waves in free space respectively. The calculated  $d_m$  based on equation (6) is shown in figure 11(b), which is well consistent with the  $d_m$  obtained from the RL results. Thus, the attenuation peaks of the BCN/Fe<sub>x</sub>(B/C/N)<sub>y</sub> nano-architectures shift to low frequency with increasing the sample thickness. And this result indicates that quarter-wavelength absorption is another effective way to improve EM wave absorption for the designed nanostructures except for the intrinsic dielectric loss.

Experimental spectrum of dielectric permittivity and loss tangent over the high frequency range exhibits obvious fluctuation (figure 9), suggesting strong multiple loss mechanisms occurred. Firstly, the migration of free electrons located in conductive carbon lattice which were excited by external electric field is responsible for the electric polarization. And the relaxation loss originated from polarization process would be enhanced by the incorporation of polar B–C, N–C bonds

and defects, which is also accordance with the increasing in real permittivity. Secondly, relaxation loss originated from hopping migration of electrons among defects also makes contribution to overall EM wave absorbing performance. Finally, as demonstrated in figure 11, quarter-wavelength absorption plays a dominated role in enhancement of attenuation peaks, and is another effective way to improve EM wave absorption for the designed nanostructures except for the intrinsic dielectric loss.

## 4. Conclusion

Novel BCN/Fe<sub>x</sub>(B/C/N)<sub>y</sub> nanostructures are successfully prepared by a simple precursor annealing method. The conductive BCN nanotubes (diameter: 50–100 nm; length: 3–5 μm) with ferrite nano-dots on the cap function as absorbing unit. The Fe<sub>x</sub>(B/C/N)<sub>y</sub> shells wrapped on the BCN nanotubes function as dielectric units and the wrinkled Fe<sub>x</sub>(B/C/N)<sub>y</sub> shells (which grow with few BCN nanotubes) with paraffin function as impedance matching units. Dielectric relaxation in the hybrid binding of B–C and N–C, and quarter-wavelength absorption mechanism are proposed to explain the enhanced wave absorption property. The minimum RL can reach to -47.97 dB at 11.44 GHz with a broad bandwidth 11.2 GHz (from 3.76 to 14.96 GHz) below -10 dB indicating a competitive absorbent in stealth materials.

## Acknowledgments

This work was supported by National Natural Science Foundation of China (51302049), Natural Scientific Research Innovation Foundation in Harbin Institute of Technology (HIT.NSRIF.2015106), Technology Development Program at Weihai (2013DXGJ12), the National Key Research and Development Program of China under Grant No. 2017YFA0204600 and China Postdoctoral Science Foundation (Grant No. 2017M612996).

## ORCID iDs

Heng Luo <https://orcid.org/0000-0002-5842-6712>  
Lianwen Deng <https://orcid.org/0000-0002-4561-3068>  
Long Xia <https://orcid.org/0000-0001-7711-2201>

## References

- [1] Zhang Y *et al* 2015 Broadband and tunable high-performance microwave absorption of an ultralight and highly compressible graphene foam *Adv. Mater.* **27** 2049–53
- [2] Wang L *et al* 2014 Synthesis and microwave absorption enhancement of graphene@Fe<sub>3</sub>O<sub>4</sub>@SiO<sub>2</sub>@NiO nanosheet hierarchical structures *Nanoscale* **6** 3157–64
- [3] Sun D P, Zou Q, Wang Y P, Wang Y J, Jiang W and Li F S 2014 Controllable synthesis of porous Fe<sub>3</sub>O<sub>4</sub>@ZnO sphere decorated graphene for extraordinary electromagnetic wave absorption *Nanoscale* **6** 6557–62

- [4] Wang T, Wang H, Chi X, Li R and Wang J 2014 Synthesis and microwave absorption properties of Fe–C nanofibers by electrospinning with disperse Fe nanoparticles parceled by carbon *Carbon* **74** 312–8
- [5] Chen Y, Zhang H-B, Yang Y, Wang M, Cao A and Yu Z-Z 2016 High-performance epoxy nanocomposites reinforced with three-dimensional carbon nanotube sponge for electromagnetic interference shielding *Adv. Funct. Mater.* **26** 447–55
- [6] Zhang T, Xiao B, Zhou P, Xia L, Wen G and Zhang H 2017 Porous-carbon-nanotube decorated carbon nanofibers with effective microwave absorption properties *Nanotechnology* **28** 355708
- [7] Ji L and Zhang X 2009 Electrospun carbon nanofibers containing silicon particles as an energy-storage medium *Carbon* **47** 3219–26
- [8] Sun H *et al* 2014 Cross-stacking aligned carbon-nanotube films to tune microwave absorption frequencies and increase absorption intensities *Adv. Mater.* **26** 8120–5
- [9] Kang Y *et al* 2013 Incorporate boron and nitrogen into graphene to make BCN hybrid nanosheets with enhanced microwave absorbing properties *Carbon* **61** 200–8
- [10] Huang C *et al* 2015 Carbon-doped BN nanosheets for metal-free photoredox catalysis *Nat. Commun.* **6** 7698
- [11] Ci L *et al* 2010 Atomic layers of hybridized boron nitride and graphene domains *Nat. Mater.* **9** 430–5
- [12] Yasui H, Hirose Y, Awazu K and Iwaki M 2000 The properties of BCN films formed by ion beam assisted deposition *Colloids Surf. B* **19** 291–5
- [13] Raidongia K, Nag A, KPSS H, Waghmare U V, Datta R and Rao C N R 2010 BCN: a graphene analogue with remarkable adsorptive properties *Chem. Eur. J.* **16** 149–57
- [14] Zhang T, Zeng S F and Wen G 2014 A simple precursor pyrolysis route to BCN nanoflakes *Mater. Lett.* **132** 277–80
- [15] Sun C *et al* 2017 Metal-free ternary BCN nanosheets with synergistic effect of band gap engineering and magnetic properties *Sci. Rep.* **7** 6617
- [16] Jalaly M, Jose Gotor F, Semnan M and Jesus Sayagues M 2017 A novel, simple and rapid route to the synthesis of boron carbonitride nanosheets: combustive gaseous unfolding *Sci. Rep.* **7** 3453
- [17] Liao L *et al* 2007 Multiwall boron carbonnitride/carbon nanotube junction and its rectification behavior *J. Am. Chem. Soc.* **129** 9562–3
- [18] Iyyamperumal E, Wang S and Dai L 2012 Vertically aligned BCN nanotubes with high capacitance *ACS Nano* **6** 5259–65
- [19] Zeng S *et al* 2017 A facile approach to fabricate boron carbonnitride microspheres via precursor pyrolysis *Chem. Phys. Lett.* **674** (Suppl. C) 164–7
- [20] Lü J, Li H, Zhu P, Lü X and Li Y 2011 Composited BCN/carbon fibers prepared by hot-filament chemical vapor deposition *Appl. Surf. Sci.* **257** 4963–7
- [21] Komatsu T 2004 Bulk synthesis and characterization of graphite-like B–C–N and B–C–N heterodiamond compounds *J. Mater. Chem.* **14** 221–7
- [22] Caretti I, Jiménez I and Albella J M 2003 BCN films with controlled composition obtained by the interaction between molecular beams of B and C with nitrogen ion beams *Diam. Relat. Mater.* **12** 1079–83
- [23] Zhang J, Xie W, Xu X, Zhang S and Zhao J 2016 Structural and electronic properties of interfaces in graphene and hexagonal boron nitride lateral heterostructures *Chem. Mater.* **28** 5022–8
- [24] Li D X *et al* 2008 Synthesis of semimetallic BC<sub>3</sub>N with orthorhombic structure at high pressure and temperature *Cryst. Growth Des.* **8** 2096–100
- [25] Ma F *et al* 2017 ‘Thermal substitution’ for preparing ternary BCN nanosheets with enhanced and controllable nonlinear optical performance *J. Mater. Chem. C* **5** 2559–65
- [26] Mohammad S N 2012 Thermodynamic imbalance, surface energy, and segregation reveal the true origin of nanotube synthesis *Adv. Mater.* **24** 1262–75
- [27] Blase X, Charlier J C, DeVita A and Car R 1997 Theory of composite B<sub>x</sub>C<sub>y</sub>N<sub>z</sub> nanotube heterojunctions *Appl. Phys. Lett.* **70** 197–9
- [28] Wang L, Huang Y, Li C, Chen J and Sun X 2015 A facile one-pot method to synthesize a three-dimensional graphene@carbon nanotube composite as a high-efficiency microwave absorber *Phys. Chem. Chem. Phys.* **17** 2228–34
- [29] Ferrari A C and Basko D M 2013 Raman spectroscopy as a versatile tool for studying the properties of graphene *Nat. Nanotechnol.* **8** 235–46
- [30] Pimenta M A, Dresselhaus G, Dresselhaus M S, Cançado L G, Jorio A and Saito R 2007 Studying disorder in graphite-based systems by Raman spectroscopy *Phys. Chem. Chem. Phys.* **9** 1276
- [31] Zhi C Y, Bai X D and Wang E G 2002 Raman characterization of boron carbonitride nanotubes *Appl. Phys. Lett.* **80** 3590–2
- [32] Semenov A V, Pergament A L and Pikalev A A 2016 Raman spectroscopy of melamine-formaldehyde resin microparticles exposed to processing in complex plasma *J. Raman Spectrosc.* **47** 1293–7
- [33] Li X *et al* 2009 Large-area synthesis of high-quality and uniform graphene films on copper foils *Science* **324** 1312
- [34] Sinclair D C, Adams T B, Morrison F D and West A R 2002 CaCu<sub>3</sub>Ti<sub>4</sub>O<sub>12</sub>: one-step internal barrier layer capacitor *Appl. Phys. Lett.* **80** 2153–5
- [35] Jaiswal A, Das R, Maity T and Poddar P 2011 Dielectric and spin relaxation behaviour in DyFeO<sub>3</sub> nanocrystals *J. Appl. Phys.* **110** 124301